Contrib Mineral Petrol (1990) 105:550–561

Contributions to Mineralogy and Petrology

Trace element crystal chemistry of mantle eclogites

Florie A. Caporuscio* and Joseph R. Smyth

Department of Geological Sciences, University of Colorado, Boulder, CO 80309-0250, USA

Received November 23, 1989 / Accepted June 1, 1990

Abstract. Rare earth element (REE) concentrations have been measured using instrumental neutron activation analysis on clean separates of primary minerals from 11 eclogite samples from the Bobbejaan and Roberts Victor kimberlites, South Africa. Samples were selected to reflect minimal secondary alteration and represent a broad range of eclogite compositions from coesite- and corundum-grospydites through magnesian bimineralic eclogites. Correlations between REE concentrations and major-element compositions suggest that garnet and clinopyroxene crystal chemistry are the dominant control on REE distribution and that these approach solid-state equilibrium distributions. Reconstructed whole-rock REE concentration variation with whole-rock major-element compositions are consistent with an origin by high-pressure igneous fractionation followed by re-equilibration to lower temperatures at pressures in excess of three GPa.

Introduction

The suite of xenoliths brought to the surface by kimberlite from depths greater than 100 km is dominated by lherzolites which are olivine-rich rocks containing minor orthopyroxene, clinopyroxene, and garnet. Compositionally distinct from the lherzolite suite are mantle eclogites and associated grospydites which form a group of xenoliths of roughly basaltic composition and constitute somewhat less than 10% of all xenolith material brought to the surface by kimberlites (Dawson 1980). Mantle eclogites cover a more extended compositional range than low-pressure basalts, however, and include some very aluminous compositions that are not represented in low-pressure assemblages.

Reviews of the various hypotheses for the origin of chemical variation in these rocks are given by MacGregor and Manton (1986) and Smyth et al. (1989). These hypotheses can be divided into two main groups: (1) suggesting that eclogites are the prograde metamorphic products of seafloor basalts that had undergone igneous fractionation at low pressure and subsequent alteration at relatively low temperature prior to metamorphism (Helmstaedt et al. 1972; Smyth and Hatton 1977; Jagoutz et al. 1984; MacGregor and Manton 1986; Ongley et al. 1987; Schulze and Helmstaedt 1988; Shervais et al. 1988); (2) suggesting that eclogites are the result of igneous fractionation at high pressure and represent cumulates and evolved liquids (O'Hara andYoder 1967; Kushiro and Aoki 1968; Garlick et al. 1971; MacGregor and Carter 1971; Early 1971; Philpotts et al. 1972; Lappin and Dawson 1975; Harte and Gurney 1975; Hatton 1978; Lappin 1978; Anderson 1984; Gasparik 1984; Smyth and Caporuscio 1984; Dawson and Gurney 1987; Caporuscio 1988; Smyth et al. 1989).

The Cr-rich samples appear to form a chemically and perhaps genetically distinct group. Shervais et al. (1988) suggested that they, along with more Mg-rich and Cr-poor eclogites may be cumulates from a kimberlitic fluid. Haggerty and Sautter (1990) have observed pyroxene exsolution from garnet in the Cr-rich samples implying a super-silicious precursor garnet and suggested that they may have originated at depths greater than 300 km.

Previous studies of REE concentrations and distributions in mantle eclogites have provided useful insight, but have not covered the full range of eclogite compositions. Early (1971) measured REE abundances in whole rocks and mineral separates of bimineralic eclogites, as did Philpotts et al. (1972). Other REE compositions have also been determined by Shervais et al. (1988) and Caporuscio and Smyth (1986). Shimizu (1980) performed an experimental study of the distribution of REE between garnet, clinopyroxene, and basaltic liquid at two and three GPa and found that clinopyroxene was the liquidus phase and that garnet was difficult to nucleate in many runs.

McCormick (1984) analyzed several bimodal eclogites in which grospydites grade into bimineralic eclogites demonstrating that the two are co-genetic and intimately associated with each other. Smyth and Caporuscio (1984) reported major element analyses of a suite of about 60 eclogites from Bellsbank (Bobbejaan Mine)

* Present address: Environmental Protection Agency, New York, NY 10009, USA

Offprint requests to: J.R. Smyth

and showed that the corundum grospydites appear to form a chemically continuous series with the bimineralic eclogites. Smyth et al. (1989) used a combination of petrography, major element data, and some preliminary and previously published REE data to develop a model by which mantle eclogites evolve from grospydites to bimineralic eclogites at high pressure by igneous fractional crystallization. In order to refine and examine this model we have undertaken a careful study of REE concentrations in garnet and clinopyroxene as functions of major element compositions in these rocks. Samples selected for REE determinations in this study attempt to cover the full range of the eclogite compositional field.

It has been widely recognized that there are late-stage metasomatic and metamorphic overprints on these samples. Secondary phases (principally pyroxene, amphibole, phlogopite, spinel, and carbonates) are ubiquitous along cracks and grain boundaries of samples in the present study, and have been documented in eclogite xenoliths found worldwide (Dawson 1980). These secondary phases are considered by some authors (MacGregor and Manton 1986) to be an integral part of eclogite bulk chemistry, whereas others (Early 1971; Caporuscio and Smyth 1987) have suggested that the secondary phases may be introduced from an external metasomatizing fluid. However, Caporuscio (1988) presented data consistent with the secondary phases being introduced by later, separate MARID, kimberlite, and deuteric fluids. Because we cannot evaluate the possible effects of secondary fluids on REE compositions, it is necessary to analyze REE on clean mineral separates and to reconstruct whole-rock compositions from these data and modal analyses. Special care was taken to obtain pure, unaltered mineral-grain cores without exsolution to avoid secondary effects.

Sample selection and characterization

Xenolith population

Of some 150 samples from Bellsbank and Roberts Victor for which thin sections and major element analyses were available, 11 were chosen on the basis of minimal compositional zonation, minimal alteration, and largest variety of chemical compositions. Of the 11 samples, 2 are kyanite-bearing, and 9 are bimineralic samples spanning a range of chemical compositions (Fig. 1). One of the 9 is a Cr-rich sample Modal phase proportions are reported in Table 1. Clinopyroxene and garnet major-element analyses are listed in Tables 2 and 3, respectively.

Pyroxene

Clinopyroxenes exhibit significant compositional variation (increased acmite and Ca-Tschermaks, and decreased jadeite components) only in clearly defined rim regions that appear to be affected by secondary alteration. Clinopyroxene major-element compositions (Table 2) were cast into pyroxene end-member proportions using the computer program PYROS (Smyth 1980). Alumina contents of pyroxenes range from 1.38 wt% (SRV-4) to 17.0 wt% (SRV-1). Titanium and chromium values for pyroxene are generally <0.5 wt%, the exception being sample SBB-7P ($Cr_2O_3 =$ 3.09 wt%). Potassium ranges from zero to 0.30 wt%, with no clear gap as suggested in the group I and II classification of MacGregor and Manton (1986). End-member pyroxene components show significant variations. Jadeite values range from 5% (SRV-4) to 50% (SBB-2H). Ca-Tschermaks end-member ranges from zero to 6.8 mol% (SBB-2H), while Ca-Escola ranges from zero to 12.9% (SRV-1).

Garnet

Garnets analyzed in this study are unzoned. Garnet major-element compositions are listed in Table 3. End-member compositions range from Ca-rich (SRV-1, $Pyr_{28}Alm_{21}Grs_{51}$) to Fe-rich (SBB-39, $Pyr_{50}Alm_{37}Grs_{12}$) to Mg-rich (SBB-37, $Pyr_{76}Alm_{14}Grs_{10}$). Garnet compositions show a continuous trend from grossular(Grs) to almandine(Alm) to pyrope(Pyr)-rich compositions. Minor elements of interest are P (Z site), Ti and Cr (Y site). Titanium (as TiO_2) ranges from zero to 0.5 wt%. Chromium generally ranges 0.07–0.5 wt% oxide, the exception being sample SBB-7P with 5.50 wt% Cr_2O_3. Substitution of phosphorus for silicon (Bishop et al. 1976) is detectable (0.06–0.05 wt%) in the grossular-rich samples (SRV-1, SBB-2H), but negligible in most others. High values of spessartine end-member (3.5, 2.3 mole%) are present in samples SBB-39 and SBB-34, respectively. Garnet sodium contents range from zero to 0.08 wt%.

Other primary phases

Other primary phases observed in the suite of eclogites are kyanite, corundum, coesite, sanidine and Nb-rutile. Kyanite and corundum

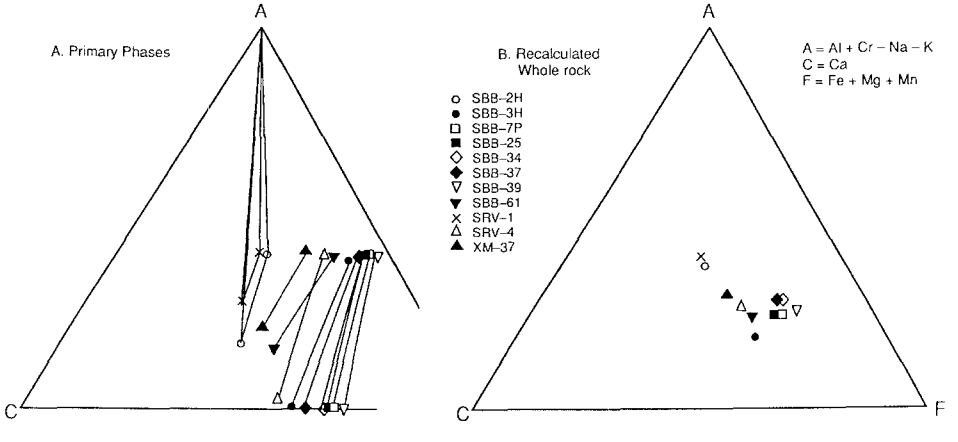

Fig. 1A, B. ACF plots of eclogite: **A** primary phases; **B** recalculated whole-rock compositions showing the range of compositions included in the sample suite

Table 1. Modal abundances of primary and secondary phases in eclogite samples selected for REE analysis

Mineral	SBB-2H	SBB-3H	SBB-7P	SBB-25	SBB-34	SBB-37	SBB-39	SBB-61	SRV-1	SRV-4	XM-37
Garnet	43	79	42	63	71	47	30	68	27	29	43
Clinopyroxene	33	19	18	34	24	38	46	29	53	63	51
Kyanite	17	–	–	–	–	–	–	–	9	–	–
Corundum	2	–	–	–	–	–	–	–	–	–	–
Coesite	–	–	–	–	–	–	–	–	5	–	–
Rutile	–	–	–	–	–	–	–	–	–	–	1
Sanidine	–	–	–	–	–	–	–	–	0.6	–	–
Secondary phases	5	2	40	3	5	15	24	3	5	8	5
Mg-number	76	63	85	69	64	85	64	70	72	83	62
K_d	6.33	3.36	3.43	2.35	2.52	2.06	2.21	3.07	5.55	4.26	3.85
T°C(3GPa)[a]	1030	936	934	1062	1040	1075	1083	1028	1087	992	1057
T°C(4GPa)[a]	1059	971	968	1101	1078	1115	1123	1064	1117	1025	1090

[a] By method of Ellis and Green (1979)

Table 2. Electron microprobe analyses of pyroxenes in eclogites selected for REE analysis

Sample	SBB-2H	SBB-3H	SBB-7P	SBB-25	SBB-34	SBB-37	SBB-39	SBB-61	SRV-1	SRV-4	XM-37
SiO_2	54.80	55.89	53.79	55.96	54.77	55.41	55.61	56.70	56.63	54.31	56.10
TiO_2	0.07	0.15	0.00	0.43	0.16	0.29	0.21	0.30	0.07	0.07	0.38
Al_2O_3	16.10	6.39	2.54	7.49	5.39	4.55	6.18	12.42	17.04	1.38	14.10
Cr_2O_3	0.03	0.05	3.09	0.19	0.09	0.18	0.10	0.09	0.04	0.00	0.15
Fe_2O_3	1.06	0.00	1.92	0.00	1.09	1.15	0.00	0.00	0.00	0.11	0.00
FeO	0.00	4.11	0.00	4.87	5.43	1.70	8.09	2.56	1.56	3.07	2.54
MnO	0.02	0.02	0.07	0.10	0.26	0.01	0.45	0.04	0.00	0.07	0.02
MgO	7.10	12.06	15.39	12.24	13.28	15.40	12.28	8.85	6.24	16.96	7.72
CaO	12.20	16.65	19.99	14.23	15.84	18.48	13.34	12.43	11.57	23.29	11.86
Na_2O	8.10	3.77	2.57	4.37	3.34	2.95	3.86	5.91	7.73	0.64	6.99
K_2O	0.00	0.00	0.01	0.08	0.16	0.00	0.11	0.07	0.20	0.11	0.29
Total	99.50	99.09	99.37	99.96	99.81	100.12	100.23	99.37	100.59	100.01	100.15
Atoms per 6 oxygens											
Si	1.924	2.017	1.958	1.999	1.985	1.981	2.008	1.997	2.011	1.969	1.966
Ti	0.002	0.004	0.000	0.012	0.004	0.008	0.006	0.008	0.002	0.002	0.010
Al^{IV}	0.072	−0.017	0.033	0.001	0.015	0.019	−0.008	0.003	0.000	0.031	0.036
Al^{VI}	0.594	0.288	0.076	0.314	0.216	0.172	0.271	0.512	0.713	0.028	0.546
Cr	0.001	0.001	0.089	0.005	0.003	0.005	0.003	0.003	0.002	0.000	0.004
Fe^{3+}	0.028	0.000	0.052	0.000	0.030	0.031	0.000	0.000	0.000	0.049	0.000
Fe^{2+}	0.000	0.124	0.000	0.145	0.165	0.051	0.244	0.075	0.045	0.047	0.074
Mn	0.001	0.001	0.002	0.003	0.008	0.000	0.014	0.001	0.000	0.002	0.001
Mg	0.372	0.649	0.835	0.652	0.718	0.821	0.661	0.465	0.329	0.917	0.403
Ca	0.459	0.644	0.780	0.545	0.615	0.708	0.516	0.469	0.440	0.905	0.445
Na	0.551	0.264	0.181	0.303	0.235	0.204	0.270	0.404	0.447	0.045	0.475
K	0.000	0.000	0.000	0.004	0.007	0.000	0.005	0.003	0.011	0.005	0.013
Vac	0.000	0.025	0.000	0.018	0.000	0.000	0.000	0.060	0.000	0.000	0.026

of sample SBB-2H are very pure. Kyanite and coesite of sample SRV-1 are also pure; sanidine analysis indicates the highest K content for any natural feldspar (Smyth and Hatton 1977; Scambos et al. 1987). Rutile of sample XM-37 has appreciable Nb (3–5 wt%) but this element was not quantitatively analyzed.

Analytical techniques

Mineral separation

A portion of each sample was coarse-crushed with a carbide steel piston sleeve assembly and then split into two fractions. The first split was set aside for future studies. The second sample split was then used to obtain pure mineral separates of kyanite, corundum, garnet, and clinopyroxene. The object of mineral separation was to obtain mineral-grain cores devoid of secondary alteration effects. Hand-picking of separates using a binocular microscope (7–30 × magnification) was used to avoid heavy liquid contamination. After coarse crush (20 mesh), grains picked were rinsed in pure H_2O, immersed in warm HCl to remove trace carbonates, and inspected for impurities at high magnification in oil immersion. Grains were then rinsed in reagent-grade acetone to remove oil, and then H_2O to remove traces of acetone. Pure grains were then set aside, those with alteration were returned to the selection pile for further crushing. This process was repeated at 50, 75, 100 mesh

Table 3. Electron microprobe analyses of garnets in eclogites selected for REE analysis

Sample	SBB-2H	SBB-3H	SBB-7P	SBB-25	SBB-34	SBB-37	SBB-39	SBB-61	SRV-1	SRV-4	XM-37
SiO_2	40.60	41.69	41.21	41.89	41.48	42.46	40.36	42.10	40.31	40.52	39.66
TiO_2	0.05	0.13	0.00	0.30	0.16	0.16	0.21	0.20	0.17	0.48	0.46
Al_2O_3	22.50	22.86	19.47	22.63	22.18	23.36	21.37	22.77	21.94	21.48	22.48
Cr_2O_3	0.07	0.10	5.50	0.16	0.14	0.23	0.14	0.06	0.14	0.53	0.00
FeO	7.80	16.25	7.51	14.66	16.78	7.97	19.57	13.17	10.25	11.30	15.20
MnO	0.18	0.28	0.58	0.40	1.12	0.47	1.67	0.30	0.29	0.30	0.52
MgO	10.00	14.17	19.66	15.70	14.48	21.69	13.43	14.94	7.57	14.24	10.19
CaO	18.30	4.91	5.32	3.92	4.32	3.62	3.64	7.17	18.90	10.88	11.72
Na_2O	0.00	0.00	0.01	0.04	0.05	0.07	0.08	0.07	0.07	0.00	0.00
K_2O	0.00	0.00	0.00	0.00	0.00	0.00	0.00	0.01	0.00	0.00	0.00
P_2O_5	0.06	0.00	0.01	0.00	0.00	0.00	0.00	0.05	0.05	0.02	0.00
Total	99.56	100.39	99.27	99.70	100.71	100.03	100.47	100.84	99.69	99.75	100.27
Atoms per 12 oxygens											
Si	2.998	3.044	2.994	3.053	3.038	2.996	3.013	3.039	3.016	2.986	2.962
Ti	0.003	0.007	0.000	0.016	0.009	0.008	0.012	0.011	0.008	0.027	0.026
Al	1.958	1.967	1.667	1.944	1.914	1.942	1.880	1.937	1.935	1.863	1.979
Cr	0.004	0.006	0.316	0.009	0.008	0.013	0.008	0.003	0.008	0.031	0.000
Fe	0.482	0.992	0.456	0.893	1.028	0.470	1.222	0.795	0.641	0.696	0.950
Mn	0.011	0.017	0.036	0.025	0.070	0.028	0.106	0.018	0.017	0.019	0.033
Mg	1.011	1.543	2.129	1.706	1.581	2.282	1.495	1.608	0.845	1.562	1.135
Ca	1.448	0.384	0.414	0.306	0.339	0.274	0.291	0.554	0.516	0.858	0.938
Na	0.000	0.000	0.001	0.006	0.007	0.010	0.012	0.010	0.013	0.000	0.000
K	0.000	0.000	0.000	0.000	0.000	0.000	0.000	0.000	0.000	0.000	0.000
P	0.005	0.000	0.001	0.000	0.000	0.000	0.000	0.003	0.000	0.000	0.000
Total	7.985	7.962	8.014	7.957	7.995	8.023	8.037	7.980	7.999	8.042	8.023
X_{Ca}^{GT}	0.492	0.132	0.138	0.105	0.115	0.090	0.097	0.187	0.504	0.286	0.312

until sufficient amounts were obtained for REE analyses. The relatively coarse grain-size facilitated transferal from sealed glass tubes to plastic vials without loss of fine material.

Instrumental neutron activation analyses

Garnet and clinopyroxene separates were analyzed along with two kyanite (SRV-1, SBB-2H) and one corundum (SBB-2H) separates. All samples were irradiated for 8 h at 10 MW in the University of Missouri (Columbia), Research Reactor facility. Use of a polyethylene lazy susan ensured uniform flux, equal to 4.9×10^{13} neutrons/cm^{-2} s^{-1}. Sample emissions were then counted 3 times for a period of 4 h each, using two detectors. A 30 cm^3 lithium-drifted germanium coaxial gamma-ray detector, was used first since samples could be located from 1–35 cm away. Then, two count times were performed with the second detector, a NaI crystal and intrinsic Ge semiconductor. Natural rock standards (NBS basalt 688 and CRB-1 basalt glass) were used both for calibration and internal check of accuracy.

Results

Clinopyroxene

REE values for clinopyroxene are listed in Table 4, and representative chondrite-normalized values are plotted in Fig. 2. Pyroxenes show L(light)-REE enrichment and H(heavy)-REE depletion. Values of La/Yb range from 223 (sample SBB-7P) to 5.6 (sample SBB-34). There is commonly an increase in chondrite-normalized components from La to Ce and Nd such that the trend from LREE to HREE is not strictly linear. The overall patterns are similar to clinopyroxene REE trends described for other high-pressure eclogitic pyroxenes (Shervais et al. 1988, Early 1971). The two grospydite pyroxene samples have similar patterns with peculiar M(middle)-REE enrichments (Nd, Eu) and a slight Sm-depletion. Some authors (Shervais et al. 1988; MacGregor and Manton 1986) have suggested these MREE enrichments to be positive Eu anomalies, however, careful inspection indicates that at least four of the REE are affected by this phenomenon. Further, there is an inverse correlation between jadeite component of the pyroxenes and total REE content. Sample SBB-37 has the highest total REE content and is relatively jadeite-poor (15 mol%), whereas sample SBB-2H with 46 mol% jadeite has very low total REE.

Garnet

Garnet REE values are listed in Table 5. Three representative, chondrite-normalized garnet REE patterns (Fig. 2) do not consistently exhibit a linear trend from LREE depletion to HREE enrichment seen in Mg-rich garnets from peridotitic samples (Dawson 1980). All La/

Table 4. Neutron activation analyses (ppm) of pyroxenes in eclogites selected for REE analysis

Sample	SBB-2H	SBB-3H	SBB-7P	SBB-25	SBB-34	SBB-37	SBB-39	SBB-61	SRV-1	SRV-4	XM-37
La	0.835	3.37	7.96	2.06	1.44	9.62	1.13	2.12	0.477	4.55	0.684
Ce	1.52	6.870	26.3	6.23	5.22	33.9	4.08	5.90	1.06	13.2	2.39
Nd	0.585	2.34	18.5	5.07	4.83	24.9	3.58	4.15	1.05	8.94	2.09
Sm	0.044	0.456	4.17	1.22	1.15	5.03	0.922	0.797	0.165	1.42	0.583
Eu	0.030	0.232	0.955	0.372	0.373	1.44	0.266	0.232	0.085	0.272	0.151
Tb	0.026	0.079	0.161	0.087	0.137	0.457	0.092	0.066	0.010	0.057	0.035
Dy	0.233	0.469	1.61	0.733	0.661	3.39	0.797	0.598	0.390	0.329	0.210
Yb	0.018	0.092	0.035	0.093	0.259	0.358	0.152	0.029	0.012	0.021	0.025
Lu	0.003	0.011	0.006	0.010	0.034	0.035	0.018	0.005	0.003	0.004	0.002
La/Yb	46.9	36.6	223	22.1	5.6	26.9	7.5	72.7	41.5	216.4	27.6
ΣREE[a]	3.06	13.44	58.09	15.14	13.44	75.08	10.24	13.29	2.86	28.46	5.96
ΣREE[b]	1.54	6.34	30.85	8.54	7.85	40.45	5.89	7.16	1.72	14.99	3.42

[a] Sum of all REE analyzed; [b] Sum of all REE analyzed exclusive of Ce

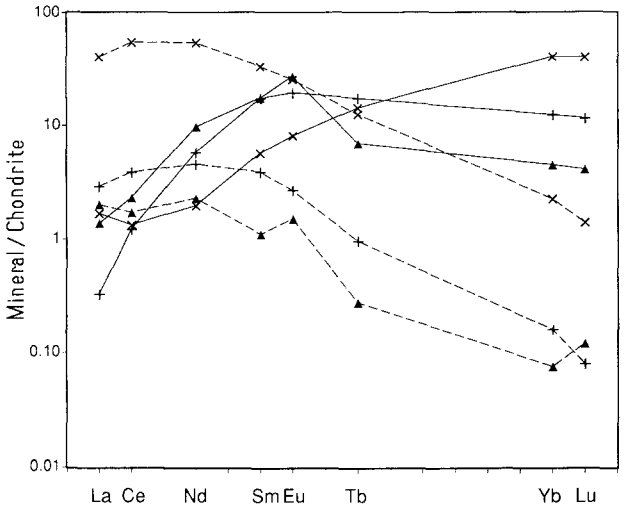

Fig. 2. Chondrite-normalized REE concentrations of garnets (*solid lines*) and clinopyroxenes (*dashed lines*) from three representative eclogites: a grospydite, SRV-1(▲) ($Grs_{50}Alm_{22}Pyr_{28}$ and Jd_{46}; XM-37(+) ($Grs_{31}Alm_{32}Pyr_{37}$ and Jd_{39}); SBB-37(×) ($Grs_{09}Alm_{12}Pyr_{79}$ and Jd_{19}). Note the shift in the shape of the garnet pattern with changing Ca-content and the declining total REE concentration of the pyroxene with increasing Na-content

Yb ratios are <1, indicating relative HREE enrichment. Values of this ratio range from 0.027 (SBB-39) to 0.70 (SBB-7P). In detail, these eclogitic garnets show significant variations in REE trends associated with major-element compositions (Fig. 2). The most pyrope-rich garnet (SBB-37, Pyr_{76}) is very similar in REE distribution to peridotitic garnets (HREE = 40 × chondrite, LREE = 1.5 × chondrite). As garnet compositions increase in Fe and Ca (XM-37), there is a flattening of the HREE and increase of the MREE portion of the patterns. Calcic garnets (SRV-1 Grs_{50}) exhibit marked MREE enrichment, but LREE and HREE depletions. Sample SBB-7P, with a high pyrope content (Pyr_{71}) and equivalent almandine-grossular components (14.5 mol%) has a chondrite normalized REE pattern similar to Fe-rich eclogitic garnets. Sample SBB-3H has a significant Fe component (Alm_{34}), but a still greater Mg component (Pyr_{53}) and displays an Mg-rich garnet REE pattern.

Garnet crystals in the eclogites exhibit virtually no zoning of major elements from core to rim. Clinopyroxenes are also free of systematic zoning, exhibiting chemical variations only at the very rims of the crystals. This variation in the pyroxene-rim chemistry appears to be

Table 5. Neutron activation analyses (ppm) of garnets in selected eclogites

Sample	SBB-2H	SBB-3H	SBB-7P	SBB-25	SBB-34	SBB-37	SBB-39	SBB-61	SRV-1	SRV-4	XM-37
La	0.224	0.107	0.576	0.563	0.320	0.398	0.082	0.995	0.326	0.184	0.077
Ce	0.644	0.381	2.05	1.26	0.895	0.827	0.360	1.85	1.42	2.015	0.759
Nd	0.397	0.642	4.85	0.653	0.395	0.905	0.301	1.81	4.47	4.79	2.65
Sm	0.179	0.215	1.88	0.580	0.461	0.854	0.409	1.42	2.63	2.94	2.62
Eu	0.148	0.206	0.843	0.266	0.269	0.456	0.190	0.708	1.53	1.10	1.10
Tb	0.090	0.291	0.418	0.233	0.299	0.521	0.275	0.461	0.252	0.613	0.632
Dy	1.01	0.136	0.906	1.56	1.95	3.73	0.266	2.24	1.41	0.797	3.34
Yb	0.522	2.71	0.824	1.80	4.88	6.55	3.07	1.66	0.715	1.812	2.00
Lu	0.071	0.429	0.128	0.272	0.804	1.02	0.493	0.239	0.103	0.267	0.294
La/Yb	0.430	0.040	0.700	0.310	0.066	0.061	0.027	0.600	0.460	0.100	0.039
La/Yb_n	0.28	0.03	0.45	0.21	0.04	0.04	0.02	0.39	0.30	0.07	0.02
La/SM_n	0.76	0.30	0.18	0.60	0.43	0.27	0.12	0.42	0.08	0.04	0.02
Tb/Yb_n	0.90	0.57	2.70	0.69	0.33	0.42	0.47	1.46	1.86	1.78	1.07

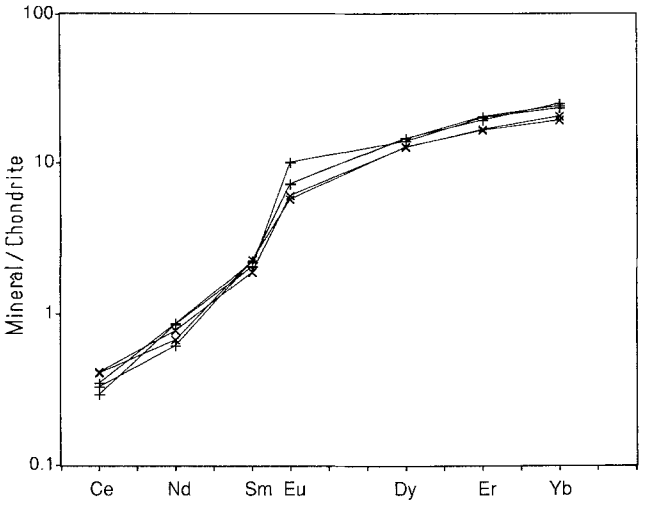

Fig. 3. Chondrite-normalized REE concentrations of five garnets, two coarse grains (×), and three exsolution lamellae (+) from sample SBB-3H ($Grs_{50}Alm_{22}Pyr_{28}$). Identical platterns indicate that equilibrium distributions have been attained

due to reaction with external fluids (Early 1971; Erlank 1970). Equilibration of major elements appears complete even down to the garnet lamellae in sample SBB-3H. This sample has large garnet crystals abutting pyroxenes and a few of the pyroxenes contain garnet lamellae. The major-element compositions of large garnet grains and physically separate garnet lamellae in pyroxene are identical within statistical error. In order to examine the extent of REE equilibration we examined these garnets in the ion microprobe.

In collaboration with Dr. P. Bottazzi at the University of Pavia we used the ion microprobe to measure REE concentrations of a large garnet grain and garnet lamellae within a clinopyroxene grain of sample SBB-3H. The concentrations are depicted in Fig. 3 and indicate that the REE values are identical. These REE values suggest that although the two types of garnet formed at different times and are physically separated within the sample, the REE have diffused and equilibrated under mantle conditions. The lack of significant major- or trace-element zoning even in exsolved samples indicates that these rocks have approached equilibrium distributions of these elements at mantle conditions.

Primary accessory phases

The primary phases kyanite, corundum, and coesite contain insignificant amounts of REE and therefore are not listed. Sanidine could not be analyzed, since at less than 1 modal percent of the rock, an amount of this phase sufficient for INAA could not be separated.

Discussion

Equilibration conditions and mineral-mineral distributions

Equilibration conditions. Major-element data obtained in previous studies of these rocks indicate that they have equilibrated at pressures 3–5 GPa and temperatures 950–1250° C. The temperatures of equilibration at arbitrary pressures of 3 and 4 GPa based on the algorithm of Ellis and Green (1979) are presented in Table 1. These temperatures were computed assuming all iron to be ferrous, which is clearly not the case for SBB-7 and SRV-4, but should be a reasonable assumption for most of the other samples. The 4 GPa temperatures range from 968 to 1123° C, within the range reported for a larger suite of Bellsbank eclogites (Smyth and Caporuscio 1984). These temperatures are 300–500° C below the dry solidus temperatures estimated to be between 1450 and 1550° C at this pressure (Shimizu 1980). Smyth and Caporuscio (1984) observed no meaningful general correlations between major-element compositions and equilibration temperatures. The pressures of equilibration are difficult to estimate for the bimineralic samples, but McCormick and Smyth (1986) have reported that if kyanite is present, internally consistent estimates of pressure may be obtained from the distribution of Al between pyroxene and garnet by the method outlined by Banno (1974) and Lappin (1978). This method results in a K (equilibration constant) of 1.94 and 2.51 for samples SBB-2H and SRV-1 respectively. These pressure-sensitive curves intersect the temperature curves of Ellis and Green (1979) at 3.9 GPa and 1057° C for SBB-2H and 4.5 GPa at 1130° C for SRV-1.

Pyroxene/Garnet REE Ratios. Values of clinopyroxene REE concentrations/garnet REE concentrations are plotted against REE atomic numbers in Fig. 4. Values of La range from 1.5 to 31, Yb values 0.008–0.05. A similar range of values was reported by Philpotts et al. (1972) for a suite of Roberts Victor eclogites. The patterns show similarities consistent with a common mode of equilibration. All samples in Fig. 4 have similar slopes, at least for Nd through Lu. There is also a positive correlation between major-element compositions of the samples and clinopyroxene/garnet REE ratios. High values correlate with Mg-rich samples, whereas low ratios belong to Ca-rich eclogites. The smoothness of the patterns and their placement in Fig. 4, together with the lack of significant major-element zoning and trace-element zoning in at least one sample, all suggest that the REE approach their equilibrium distributions between garnet and clinopyroxene in these samples.

Clinopyroxene crystal chemistry. Chondrite-normalized REE patterns of the 11 clinopyroxene samples show that the 9 bimineralic eclogites exhibit smoothly decreasing trends from the LREE to the HREE, consistent with the expected slope of partition coefficients reported by Irving and Frey (1978) and Green and Pearson (1985). Samples exhibiting exsolution (SBB-2H, SBB-3H) are both Ca-, Al-rich clinopyroxenes and display marked MREE enrichments. Experimental partition-coefficient determinations for sodic pyroxenes crystallizing alone from a basaltic melt at three GPa reflect a similar MREE enrichment (e.g., sample D-A-30-73, Shimizu 1980).

In order to evaluate the various crystal-chemical factors controlling trace-element distributions in these

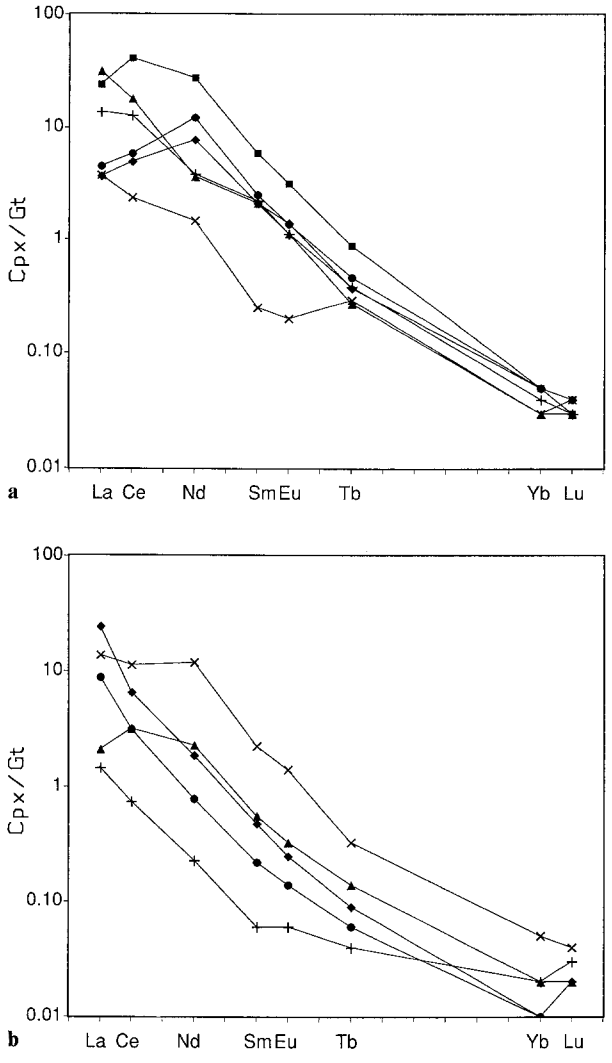

Fig. 4. **a** Plot of clinopyroxene-garnet distribution ratios for various lanthanides. Peak near Nd occurs for samples with high grossular garnets. Lowest ratios occur for samples with high jadeite-content pyroxenes. SBB-2H(×), SBB-3H(▲), SBB-7P(+), SBB-25(◆), SBB-34(●), SBB-37(■). **b** Plot of clinopyroxene-garnet distribution ratios for various lanthanides. Peak near Nd occurs for samples with high grossular garnets. Lowest ratios occur for samples with high jadeite-content pyroxenes. SBB-39(×), SBB-61(▲), SRV-1(+), SRV-4(◆), XM-37(●)

rocks, we have characterized the various cation sites available in these phases. Cation-site radii and optimal cation charges for the three cation sites in clinopyroxenes of various compositions are presented in Table 7. The site radius is taken as mean cation-oxygen distance minus the 0.14 nm assumed radius for oxygen. The optimal cation charge Q_{opt} was computed by linear regression from the empirical relationship between site potential and nominal cation charge:

$$Q_{opt} = P/11.6$$

where P is the site electrostatic potential in volts (Smyth and Bish 1988). Over the composition range represented in the current suite of clinopyroxenes, the M2-site radius varies by less than 3%, whereas the optimal cation charge for this site varies by about 22%. The radii and optimal charges of the pyroxene M1 site varies by similar factors in both radius and charge, but the Si sites vary by much smaller amounts. Since M2 is the only site that can accept appreciable REE, we expect to see an inverse correlation of total REE concentrations in pyroxene with Na content but relatively little variation with composition in qualitative fractionation patterns of pyroxene relative to coexisting garnet.

Figure 5 which plots Σ REE* (sum of analyzed trivalent REE) vs jadeite content, confirms these trends. The most sodic pyroxenes (Ca, Al-rich grospyditic pyroxenes) have very high jadeite content and low Σ REE*. The correlation of increasing Ca in M2 (lessening of jadeite component) and increase of Σ REE* (Σ REE* = −0.3 Jd + 16.88) is very good for 9 of the 11 samples. The total REE concentration in sample SBB-7 P is not consistent with these trends and may be related to the sample's extreme Cr_2O_3 content (3.09 wt%). Shervais et al. (1988) suggest that the Cr-rich and olivine-bearing samples may have a different origin from the rest of the suite, being igneous cumulates from a kimberlitic liquid. In summary, there is substantial geochemical evidence to suggest that the Σ REE* concentration of eclogitic pyroxenes is dependent on charge-balance considerations involving the Na-bearing component jadeite.

Garnet crystal chemistry. Chondrite-normalized REE patterns of the garnets are shown in Fig. 2. Substitution of the REE occurs in the 8-coordinated X cation site in garnet (Meagher 1980). For the samples of this study, concentrations of the REE appear to vary with the dominant divalent cation (Ca, Mg, Fe) in the X site (Smyth 1984). Figure 2 shows that pyrope-rich garnets are HREE enriched and similar to lherzolitic garnets in both trend and magnitude. However, Fe- and Ca-rich garnets do not appear similar to any previously reported igenous samples (Irving and Frey 1978). As with previous results for major elements, the observed REE patterns do not appear consistent with simple fractionation of garnet from a MORB-like liquid, but rather reflect re-equilibration at temperatures substantially below the solidus and are controlled by the competing crystal chemistries of the garnet and pyroxene.

In order to evaluate the crystal-chemical control on REE distributions in garnet, cation-site radii and optimal cation charges for the three cation sites in garnets of various compositions were calculated and are presented in Table 8. In contrast to the clinopyroxenes in these rocks, the radius appeared to have greater effect than the site potentials. Over the composition range represented in the current suite of garnets, the X-site radius varies by more than 10%, whereas the optimal cation charge for this site varies by only about 6%. The radii and optimal charges of the other garnet sites vary by much smaller amounts. Based on these values we expect that the total REE values for the garnets should not show much variation with composition, but that the optimum radius might show significant variation.

Figure 6a shows chondrite-normalized La/Sm ratios (La/Sm_n) vs percent grossular component in garnet.

Table 6. Recalculated whole-rock major (wt%) and trace (ppm) element compositions for eclogites selected for REE analysis

Sample	SBB-2H	SBB-3H	SBB-7P	SBB-25	SBB-34	SBB-37	SBB-39	SBB-61	SRV-1	SRV-4	XM-37
SiO_2	44.0	44.5	45.0	46.8	44.8	48.3	49.5	46.5	52.7	49.9	48.9
TiO_2	0.05	0.13	0.00	0.35	0.16	0.22	0.21	0.23	0.09	0.20	0.45
Al_2O_3	29.0	19.6	14.4	17.3	18.0	14.9	12.3	19.7	21.4	7.81	18.3
Cr_2O_3	0.03	0.09	5.33	0.17	0.13	0.21	0.12	0.07	0.07	0.17	0.00
FeO	3.88	13.8	5.80	11.2	14.2	5.64	12.7	9.99	3.77	5.77	8.33
MnO	0.09	0.23	0.49	0.30	0.91	0.26	0.94	0.22	0.08	0.14	0.23
MgO	6.99	13.8	18.4	14.5	14.2	18.9	12.7	13.1	5.62	16.1	8.40
CaO	12.5	7.26	9.72	7.53	7.20	10.3	9.46	8.75	11.8	19.3	11.8
Na_2O	2.84	0.75	0.78	1.56	0.87	1.37	2.35	1.82	4.35	0.44	3.34
K_2O	0.00	0.00	0.00	0.03	0.04	0.00	0.07	0.02	0.21	0.07	0.20
Total	99.4	100.1	99.9	99.9	100.5	100.1	100.3	100.4	100.1	99.9	99.9
Sc	14.1	36.9	90.2	38.2	59.4	58.5	29.5	35.2	9.05	67.7	18.8
Rb	1.00	0.88	2.08	1.95	2.50	0.88	0.67	2.26	2.54	0.78	0.66
Sr	17.8	40.0	98.8	28.8	78.9	164.0	120.0	90.8	150.9	56.2	413.0
Zr	5.54	23.2	101.0	24.8	15.6	49.1	15.4	36.2	17.5	28.3	56.3
Cs	0.22	0.19	0.34	0.11	0.16	0.16	0.83	0.54	0.27	0.07	0.18
Ba	519.0	12.6	33.3	117.0	15.3	25.9	13.4	192.0	1670.0	19.7	25.3
La	0.393	0.759	2.79	1.09	0.600	4.55	0.713	1.33	0.358	3.15	0.411
Ce	0.821	1.68	9.32	3.00	1.98	15.7	2.59	3.07	0.991	9.62	1.66
Nd	0.383	0.982	8.95	2.20	1.50	11.7	2.27	1.24	1.84	7.61	2.34
Sm	0.096	0.263	2.57	0.804	0.634	2.74	0.717	1.23	0.828	1.91	1.50
Eu	0.077	0.211	0.877	0.303	0.295	0.899	0.235	0.565	0.477	0.537	0.578
Tb	0.050	0.249	0.341	0.182	0.259	0.492	0.165	0.343	0.076	0.235	0.304
Dy	0.537	0.203	1.12	1.27	1.63	3.58	0.585	1.75	0.614	0.479	1.62
Yb	0.241	2.19	0.587	1.20	3.73	3.76	1.32	1.19	0.207	0.594	0.912
Lu	0.451	0.345	0.091	0.180	0.611	0.578	0.208	0.169	0.031	0.088	0.134
Hf	0.193	0.095	0.811	0.744	0.800	1.30	0.498	0.737	0.819	0.314	1.68

Table 7. Characteristics of cation sites in clinopyroxene

Pyroxenes	Diopside[a]	CaTs[b]	$Jd_{60}Di_{20}Hd_7CEs_{13}$[c]	Jadeite[a]
M2 Site				
Radius (pm)	109.8	106.0	107.7	106.9
Potential (v)	−20.77	−21.14	−16.96	−13.57
Ideal Chg.	1.79	1.83	1.46	1.17
M1 Site				
Radius (pm)	67.7	54.7	56.3	52.9
Potential (v)	−27.86	−37.45	−33.79	−37.43
Ideal Chg.	2.41	3.23	2.92	3.23
Si Site				
Radius (pm)	23.5	28.5	23.0	22.5
Potential (v)	−47.67	−42.58	−47.81	−48.17
Ideal Chg.	4.12	3.68	4.13	4.16

[a] Cameron et al. (1973); [b] Okamura et al. (1974); [c] McCormick (1986)

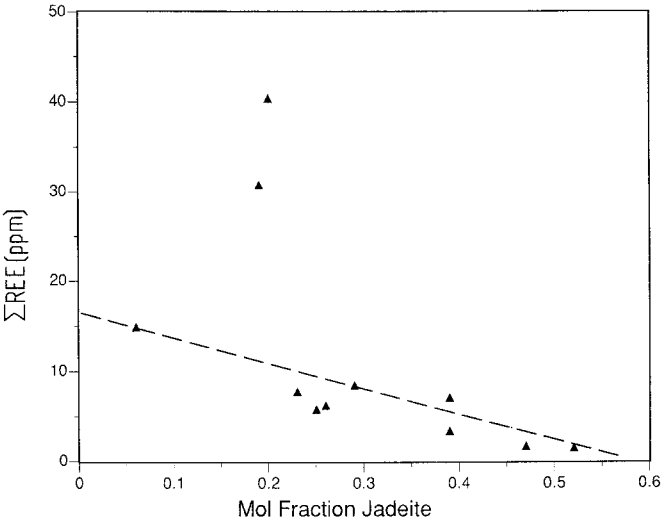

Fig. 5. A plot of total (analyzed) REE (ppm) (ΣREE) vs mole fraction of jadeite in clinopyroxenes. A strong trend of decreasing ΣREE* with increasing jadeite above 20 mol% is evident. All but two of the data points lie close to the linear regression line; ΣREE* = 16.9–30 Jd

High-Mg garnets (SBB-25) have La/Sm_n values of 0.6, indicating small enrichment of the MREE. As one progresses to more Ca-rich garnets, one sees a systematic enrichment in the MREE concentrations. This is in agreement with how the REE patterns change in Fig. 2. Figure 6b is a plot of Tb/Yb_n ratios vs grossular component. In this diagram, Mg-rich samples are HREE enriched and MREE depleted. As Ca increases in the X site there is a corresponding increase in the MREE relative to the HREE. This is also in agreement with the analytical results (Fig. 2). Preferential partitioning of larger-radius MREE into grossular garnets can thus be

Table 8. Characteristics of cation sites in garnet

Garnets	Pyrope[a]	Almandine[a]	$Grs_{50}Pyr_{28}Alm_{22}$[b]	Grossular[a]
X Site				
Radius (pm)	97.0	89.9	95.9	100.5
Potential (V)	−24.43	−23.88	−22.84	22.17
Ideal Chg.	2.11	2.06	1.97	1.91
Y Site				
Radius (pm)	48.7	49.6	49.5	52.4
Potential (V)	−38.56	−38.40	−38.80	−38.18
Ideal Chg.	3.33	3.32	3.35	3.30
Z Site				
Radius (pm)	23.5	22.8	23.7	24.5
Potential	−47.51	−47.87	−47.81	47.75
Ideal Chg.	4.10	4.13	4.13	4.12

[a] Novak and Gibbs (1971); [b] Smyth and Bish (unpublished)

attributed to cation-site radius controls (Caporuscio and Smyth 1986). However, sample SBB-2H falls significantly off the trend in Fig. 6b. The cause of this is not readily apparent but there may have been some grain-boundary contamination or the compositions may have been affected by metasomatism prior to equilibration.

Whole-rock compositions

Modal analyses of primary phases (Table 1) were used to compute estimated whole-rock compositions of both major and trace elements (Table 6). In major elements, the bimineralic samples roughly resemble mid oceanic ridge basalts, except that the eclogites have much lower TiO_2 and K_2O contents. The coesite grospydite (SRV-1) resembles an anorthosite in bulk composition, whereas the corundum grospydite (SBB-2H) is too high in alumina and too low in K to resemble any crustal rock. Interestingly, the apparent Ti and K depletion of the bimineralic samples may disappear if the secondary assemblage is included. Also, the secondary assemblages of the grospydites and the bimineralic eclogites are distinct in both mineralogy and composition even when they occur juxtaposed in the same rock (McCormick et al. 1989; McCormick and Smyth 1990).

As outlined earlier, two major hypotheses for the origin of chemical variation in these rocks have been offered and discussed by numerous authors. One holds that the grospydites are the result of subduction of low-pressure plagioclase cumulates and the bimineralic samples result from subduction of oceanic basalts and gabbros. The other (Smyth et al. 1989) suggests that the grospydites may represent high-pressure igenous accumulations of liquidus hyper-aluminous pyroxenes that have undergone subsolidus re-equilibration and exsolution of kyanite and garnet. Whole-rock trace-element patterns computed from the current trace-element compositions and modal analyses (Table 6) may be able to shed some light on this question.

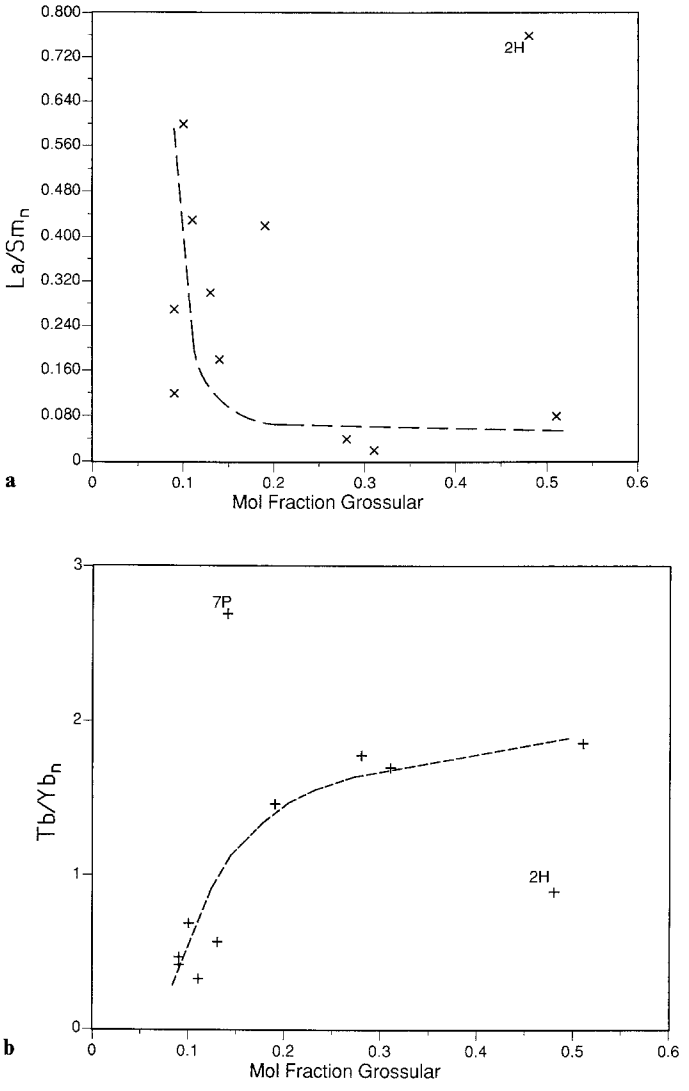

Fig. 6. a A plot of normalized La/Sm ratios vs mole fraction grossular of garnets. The trend observed suggests that MREE are accepted preferentially to LREE as the Ca content increases the radius of the X-site of garnet. The anomaly for sample SBB-2H is consistent with a small amount of contamination by LREE-rich metasomatic fluids, possibly prior to equilibration. **b** A plot of normalized Tb/Yb ratios vs mole fraction grossular of garnets. The trend observed suggests that MREE are accepted preferentially to HREE as the Ca content increases the radius of the X-site of garnet. The anomalies for sample SBB-2H and 7P are consistent with a small amount of contamination by LREE-rich metasomatic fluids, possibly prior to equilibration

From this and previous studies we expect both major and trace elements to fractionate from a liquid similarly so that both are controlled by the radius and electrostatic potential of the available cation sites in the crystal in a consistent and qualitatively predictable manner. That is, the partition coefficient should be a smooth function of both radius and charge and maxima in the partition function vs cation-radius curves (Onuma diagrams) should correspond to specific crystallographic sites. We therefore expect the composition of the liquid to affect the absolute values of the partition functions, but to have little effect on the relative values of different

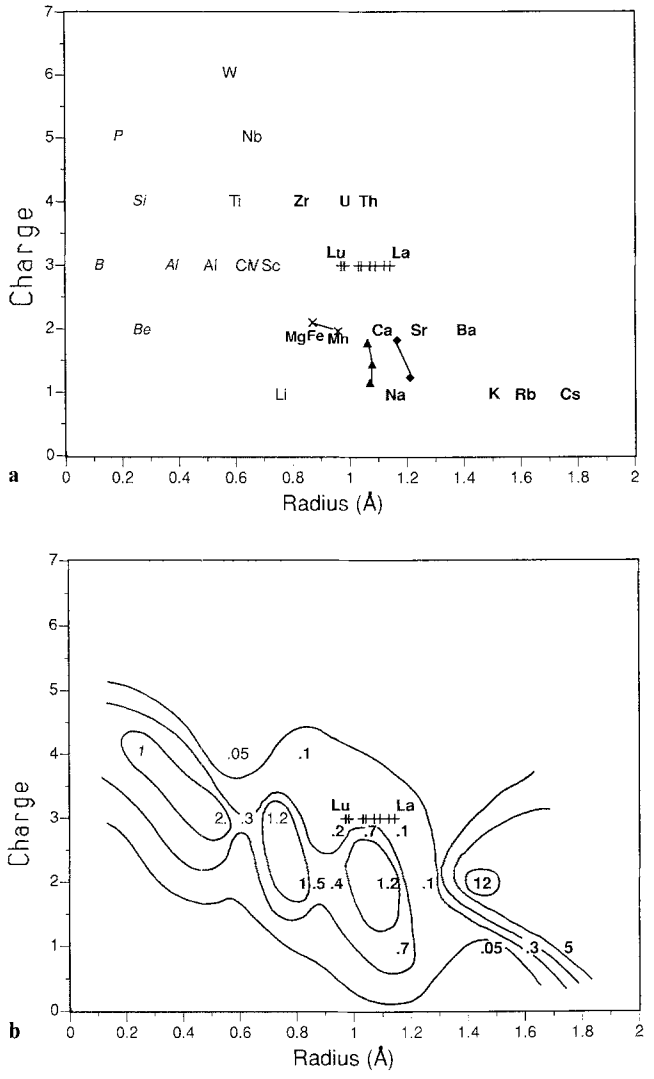

Fig. 7. **a** Radius vs charge plot for various lithophile cations in four (*italic*), six, and eight (*bold*) coordination. Also shown are the eight-fold sites in garnet (×) (Table 10), clinopyroxene (▲) (Table 9), and plagioclase (◆). **b** Radius vs charge plot for cations in reconstructed whole-rock average grospydite (samples SRV-1 and SBB-2H) with abundances ratioed to MORB KD-11 (Kay et al. 1970). Values are the *numeric ratios* for the elements identified in **a** with *italic*, *normal*, and *bold* type indicating 4, 6, and 8 coordination respectively. The partition-function surface has been roughly *contoured*

elements and thus on the radius-position of the partition-function maxima. We assume that crystal defects which are typically present at concentrations much less than 1 ppm are insignificant. If we then assume that the crystal-liquid partition function for any lithophile, homovalent cation, in major or trace concentration, is a single-valued function smooth in both radius and charge, we can construct a model based on optimal charge and radii of fractionating crystal sites, whereby we may be able to test the various hypotheses for the origin of these rocks. That is, the fractionation (accumulation) of plagioclase should be qualitatively distinguishable from that of clinopyroxene.

Figure 7a is a plot of radius vs charge for various lithophile elements in 4, 6, and 8 coordination. We have also plotted in this figure the radii and optimal charges of the various sites in clinopyroxene (Di_{100}–$Di_{50}Jd_{50}$) (Table 7), garnet (Pyr_{100}–$Pyr_{28}Alm_{22}Grs_{50}$) (Table 8), and anorthite (An_{100}) (Smyth and Bish 1988). If we assume that in this figure, the partition function for each mineral is a smooth contoured surface with maxima (ideally) at the optimal charges and radii indicated, we can predict, consistent with observation, that garnet will preferentially fractionate HREE relative to LREE and that this will change to favor lighter REE with grossular content. We can also see that clinopyroxenes will exhibit a slight MREE enrichment with an optimal radius equal to that of Eu^{3+}, and that total REE concentrations will fall off with increasing Na-contents. We can also see that plagioclase fractionation should result in slight LREE enrichments. Europium anomalies are caused by the presence of Eu^{2+} (radius 11.7 pm) and will be strongly controlled by oxygen fugacities. With or without Eu^{2+}, clinopyroxene is expected to exhibit slight Eu enrichment, but Eu enrichment would be greater in both cases under reducing conditions.

Figure 7b is a plot of the concentration of major and trace elements for the average of the two grospydites (samples SRV-1 and SBB-2H) relative to a typical MORB (KD-11 Kay et al. 1970). We can see that there is a maximum in the divalent cations at Ca and the trivalents at Eu. If the fractionation surface is contoured, the maximum is rather close to the optimal charge and radius of clinopyroxene M2 and less consistent with the radii of the divalent sites of anorthite. This is particularly true if we consider the strong depletion of Sr which shifts the maximum toward the smaller radius of M2 of pyroxene and away from the larger divalent sites of anorthite. In summary, if the grospydites were derived by plagioclase accumulation, we would expect to see a LREE enrichment, strong Eu anomaly, and slight Sr enrichment relative to a MORB-like liquid. Whereas, if they were derived by accumulation of a hyperaluminous clinopyroxene, we would expect them to show slight depletions in both light and heavy REE and slight enrichments in the middle REE including Eu, and slight depletion of Sr, which is approximately what is observed.

Further, the two grospydites, one coesite-bearing the other corundum-bearing, have very similar patterns showing much lower concentration of total REE, similar MREE enrichments, Sr depletions, and Ba enrichments. Even though they differ markedly in K and Si contents, these trace element data indicate that the two formed by a similar process.

We conclude therefore that both the trace-element patterns and major-element compositions of the grospydites are more consistent with an origin by accumulation of liquidus pyroxene at high pressures than by subduction of low-pressure accumulations of plagioclase from MORB-like basaltic liquids. The strong enrichment of the very-large-ion lithophiles, Ba and Cs, is very evident in this plot and is somewhat puzzling particularly in light of the Sr depletion. These features may be due to metasomatism that affected these samples possibly prior to equilibration, i.e., cryptic metasomatism. How-

ever, the Sr depletion and Ba- and Cs-enrichment are common to both corundum- and coesite-bearing grospydites from different localities.

Conclusions

Concentrations of major and lanthanide trace elements have been determined for garnet-clinopyroxene pairs of nine bimineralic eclogites and two grospydites from South African kimberlites. Care was taken to avoid contamination by late-stage alteration products and metasomatic phases. The observed data are consistent with effective avoidance of contamination in all cases except, possibly in samples SBB-2H garnet and SBB-7P. Major- and trace-element distributions are consistent with complete equilibration at pressures 3–5 GPa and temperatures 950–1150° C. Ion microprobe results indicate complete REE equilibration and identical compositions of two different generations of garnet: lamellae and large crystals. Although samples have equilibrated at different temperatures and pressures, the observed trace-element distributions strongly reflect systematic differences in radii and electrostatic potentials of the X site of garnet and the M2 site of clinopyroxene over the composition range studied.

Both corundum- and coesite-bearing grospydites have similar REE concentrations consistent with a similar mode of origin. Reconstructed whole-rock major- and trace-element concentrations are consistent with a derivation of the grospydites by a high-pressure igneous accumulation of hyperaluminous pyroxene from a MORB-like liquid followed by exsolution of major amounts of garnet and kyanite. The lack of light-REE enrichment in these rocks makes it unlikely that they were derived by prograde metamorphism of plagioclase-rich cumulates.

Acknowledgments. Sample XM-37 was kindly made available by the DeBeers Consolidated Mines, Ltd. Microprobe analyses were determined with the assistance of R. Hagan at Los Alamos National Laboratory. Instrumental neutron activation analyses (INAA) were done with the help of Dr. W. Boynton and D. Hill, Lunar and PLanetary Laboratory, University of Arizona. Discussions with G.L. Farmer, R. Vanucci, K. Lackner, L.A. Taylor, and I. MacGregor were extremely useful in the preparation of the manuscript. Tamsin McCormick critically reviewed the manuscript and provided some microprobe analyses. This work was supported by NSF grants EAR-87-09224 and EAR 89-04164.

References

Anderson DL (1984) Kimberlite and evolution of the mantle. In: Kornprobst J (ed) Kimberlites I: Kimberlites and related rocks. Elsevier, New York, pp 395–404

Banno S (1974) Use of partial solution of multi-component equilibria. Case study of pyroxene-bearing assemblages. Bull Soc Fr Mineral Cristallogr 97:108–116

Bishop FC, Smith JV, Dawson JB (1976) Na, P, Ti and coordination of Si in garnet from peridotite and eclogite xenoliths. Nature 260:696–697

Cameron M, Sueno S, Prewitt CT, Papike JJ (1973) High temperature crystal chemistry of acmite, diopside, hedenbergite, jadeite, spodumene, and ureyite. Am Mineral 58:594–618

Caporuscio FA (1988) Petrogenesis of mantle eclogites from South Africa. PhD dissertation, University of Colorado (Boulder), Colo, USA

Caporuscio FA, Smyth JR (1986) Trace element compositions of mineral separates from mantle eclogites. Trans Am Geophys Union 67:1253

Caporuscio FA, Smyth JR (1987) Variable LREE enrichment of mantle eclogites from South Africa by MARID fluids (abstracts program). Geol Soc Am 19:250

Dawson JB (1980) Kimberlites and Their Xenoliths. Springer, Berlin Heidelberg New York

Dawson JB, Gurney JJ (1987) Roberts Victor eclogites and their relations to the mantle. In: Nixon PH (ed) Mantle Xenoliths. Wiley and Sons Ltd., pp 453–463

Early TO (1971) Rare earths in eclogites from the Roberts Victor kimberlite, South Africa. Contrib 2144, Publ Div Geol Planet Sci California Inst of Technology, Pasedena, Calif, USA

Ellis DJ, Green DH (1979) An experimental study on the effect of Ca upon garnet-clinopyroxene Fe-Mg exchange equilibria. Contrib Mineral Petrol 71:13–22

Erlank AJ (1970) Distribution of potassium in mafic and ultramafic nodules. Carnegie Inst Washington Yearb 68:233–236

Garlick GD, MacGregor ID, Vogel DE (1971) Oxygen isotope ratios in eclogites from kimberlites. Science 172:1025–1035

Gasparik T (1984) Experimentally determined stability of clinopyroxene + garnet in the system CaO-MgO-Al_2O_3-SiO_2. Am Mineral 69:1025–1035

Green TH, Pearson NJ (1985) Rare earth element partitioning between clinopyroxene and silicate liquid at moderate to high pressure. Contrib Mineral Petrol 91:24–36

Haggerty SE, Sautter V (1990) Ultra-deep (>300 km) garnet-clinopyroxene xenoliths in diamondiferous kimberlites. Trans Am Geophys Union 71:523

Harte B, Gurney JJ (1975) Evolution of clinopyroxene and garnet in an eclogite nodule from the Roberts Victor kimberlite pipe, South Africa. Phys Chem Earth 9:367–388

Hatton CJ (1978) The geochemistry and origin of xenoliths from the Roberts Victor Mine. PhD Thesis, University of Cape Town, Cape Town, South Africa

Helmstaedt H, Anderson OL, Gavasci AT (1972) Petrofabric studies in eclogite, spinel websterite, and spinel lherzolite xenoliths from kimberlite-bearing breccia pipes in southeastern Utah and northeastern Arizona. Jour Geophys Research 77:4350–4365

Irving AJ, Frey FA (1978) Distribution of trace elements between garnet megacrysts and host volcanic liquids of kimberlitic to rhyolitic composition. Geochim Cosmochim Acta 42:771–788

Jagoutz E, Dawson JB, Hornes S, Spettal B, Wänke H (1984) Anorthositic oceanic crust in the Archean. Lunar Planet Sci 15:395–396

Kay R, Hubbard NJ, Gast PW (1970) Chemical characteristics and origin of oceanic ridge volcanic rocks. J Geophys Res 75:1585–1613

Kushiro I, Aoki K (1968) Origin of some eclogite inclusions in diamond. Am Mineral 53:1347–1367

Lappin MA (1978) The evolution of a grospydite from the Roberts Victor Mine, South Africa. Contrib Mineral Petrol 66:221–241

Lappin MA, Dawson JB (1975) Two Roberts Victor cumulate eclogites and their re-equilibration. Phys Chem Earth 9:351–366

MacGregor ID, Carter JL (1970) The chemistry of clinopyroxenes and garnets of eclogite and peridotite xenoliths from the Roberts Victor Mine, South Africa. Phys Earth Planet Inter 3:391–397

MacGregor ID, Manton WI (1986) Roberts Victor eclogites: ancient oceanic crust. J Geophys Res 91:14063–14079

McCormick TC (1984) Crystal chemistry and breakdown reactions of aluminous mantle-derived omphacites. PhD dissertation, Arizona State University, Tempe, Ariz, USA

McCormick TC (1986) Crystal-chemical aspects of non-stoichiometric pyroxenes. Am Mineral 71:1434–1440

McCormick TC, Smyth JR (1986) Geothermometry and geobarometry for kyanite eclogites from Bellsbank and Roberts Victor kimberlites (abstracts program). Int Mineral Assoc 14:169

McCormick TC, Smyth JR (1990) Petrology of secondary phases in mantle eclogites. Trans Am Geophys Union 71:524

McCormick TC, Smyth JR, Caporuscio FA (1989) Banded eclogite xenoliths: some constraints on chemical equilibration and metasomatism in the mantle. Trans Am Geophys Union 70:1411

Meagher EP (1980) Silicate garnets. Rev Mineral 5:25–112

Novak GA, Gibbs GV (1971) The crystal chemistry of the silicate garnets. Am Mineral 56:791–825

O'Hara MJ, Yoder HS (1967) Formation and fractionation of basic magmas at high pressures. Scott J Geol 3:67–117

Okamura FP, Ghose S, Ohashi H (1974) Structure and crystal chemistry of calcium Tschermaks pyroxene $CaAlAlSiO_6$. Am Mineral 59:549–557

Ongley JS, Basu AR, Kyser TK (1987) Oxygen isotopes in coexisting garnets, clinopyroxenes, and phlogopites from Roberts Victor eclogites: implications for petrogenesis and mantle metasomatism. Earth Planet Sci Lett 83:80–84

Phillpotts JA, Schnetzler GC, Thomas HM (1972) Petrogenetic implications of some new geochemical data on eclogite and ultrabasic inclusions. Geochim Cosmochim Acta 36:1131–1166

Scambos TA, Smyth JR, McCormick TC (1987) Crystal structure refinement of high sanidine from the upper mantle. Am Mineral 72:973–978

Schulze DJ, Helmstaedt H (1988) Coesite-sanidine eclogites from kimberlite: products of mantle fractionation or subduction? J Geol 96:435–443

Shervais JW, Taylor LA, Lugmair GW, Clayton RN, Mayeda TK, Korotev RL (1988) Early Proterozoic oceanic crust and the evolution of subcontinental crust: Eclogites and related rocks from southern Africa. Geol Soc Am Bull 100:411–423

Shimizu H (1980) Experimental study on REE partitioning in minerals formed at 20 and 30 Kb as for basaltic systems. Geochem J 14:185–202

Smyth JR (1980) Cation vacancies and the crystal chemistry of breakdown reactions in kimberlitic omphacites. Am Mineral 65:1257–1264

Smyth JR (1984) Middle-rare-earth enrichment in mantle-derived eclogitic garnets (abstract). Trans Am Geophys Union 65:306

Smyth JR, Bish DL (1988) Crystal structures and cation sites of the rock-forming minerals. Allen and Unwin, Boston-London-Sydney-Wellington

Smyth JR, Caporuscio FA (1984) Petrology of a suite of eclogite inclusions from the Bobbejaan kimberlite: II. Primary phase compositions and origins. In: Kornprobst J (ed) Kimberlites II: The mantle and crust-mantle relationships. Elsevier, Amsterdam, pp 121–132

Smyth JR, Hatton CJ (1977) A coesite-sanidine grospydite from the Roberts Victor kimberlite. Earth Planet Sci Lett 34:284–290

Smyth JR, Caporuscio FA, McCormick TC (1989) Mantle eclogites: evidence of igneous fractionation in the mantle. Earth Planet Sci Lett 93:133–141

Editorial responsibility: T. Grove